

Damping and excitation variations of the solar acoustic modes using LOWL observations

D. Salabert*

*High Altitude Observatory, National Center for Atmospheric Research, P.O. Box 3000,
Boulder, CO 80307-3000, USA*

and

S.J. Jiménez-Reyes

Instituto de Astrofísica de Canarias, 38205 La Laguna, Tenerife, Spain

ABSTRACT

We have used observations made with the helioseismic instrument LOWL collected over ~ 6 years to carry out an independent study of the variations of the p-mode damping and excitation rates with solar activity. We observe significant variations in the mode height, mode width and mode velocity power over a wide range of angular degree values. Their sensitivities to solar activity show clear evidence of frequency dependence, the modes in the frequency range from 2700 and 3300 μHz showing the largest variations and exhibiting a maximum change centered around 3100 μHz . As for the mode energy supply rate, it is consistent, at the level of precision of the observations, with a zero change along the solar cycle and over the range of studied frequencies. Moreover, the variations with solar activity of each of these parameters are observed to be more or less ℓ -independent over the range of studied angular degrees. Our results provide the first in-depth confirmation of the findings obtained from GONG measurements for intermediate angular degrees.

Subject headings: Sun: helioseismology — Sun: activity

1. INTRODUCTION

Our knowledge and understanding of the Sun has improved considerably with the study of the solar oscillations, leading to important modifications in the solar- and stellar-evolution

*Now at: National Solar Observatory, 950 N. Cherry Avenue, Tucson AZ 85719, USA, dsalabert@nso.edu

models. Indeed, through the accurate measurements of the frequencies of acoustic modes, helioseismology has represented a revolution in solar physics, revealing a detailed picture of the structure of the Sun and its internal rotation for instance (see Thompson et al. 2003, for a detailed review). Furthermore, in the last decade, the solar p-mode parameters have also been demonstrated to be very sensitive to changes in solar activity, showing that they can also help us reach a better understanding of the processes driving the solar magnetic cycle, and of the physics of the acoustic modes themselves as, for example, the processes responsible for their excitation and damping.

The first reports about the variability of the p-mode parameters concerned the mode frequencies. Woodard & Noyes (1985) found that modes with degrees $\ell=0$ and $\ell=1$ presented a change in the central frequency of $0.42 \pm 0.14 \mu\text{Hz}$. Few years later, Duvall et al. (1988) and Libbrecht & Woodard (1990) also observed significant variations in the p-mode central frequency for intermediate degrees. The quantity of observations increasing, thanks to ground-based networks and later on space-based instruments, deeper analysis were carried out for low-degree modes (see, e.g., Chaplin et al. 1998; Jiménez-Reyes et al. 1998; Salabert et al. 2002; Gelly et al. 2002) and intermediate and high-degree modes (see, e.g., Howe et al. 1999; Jiménez-Reyes et al. 2001b), establishing, for instance, a strong ℓ -dependence in the frequency shifts. The study of the relations between the p-mode heights and widths with the solar cycle is a more difficult task to achieve. Indeed, since their estimations are subject to several observational effects and that long datasets are needed, the first reports of their variabilities with solar activity were sometimes contradictory. For example, Pallé et al. (1990a) and Jefferies et al. (1990) reported an increase in mode widths with increasing activity in low- and medium- ℓ observations respectively, while no significant change were found by Elsworth et al. (1993) with full-disk data. Today, the quality and the amount of available data (some of the instruments are collecting data since more than a solar cycle) are such that it is now possible to have reliable estimates of the mode heights and widths and to study the variability with the solar cycle of the underlying p-mode damping and excitation. Recent work achieved with low- ℓ data (see, e.g., Chaplin et al. 2000; Salabert et al. 2003; Jiménez-Reyes et al. 2003) and also with intermediate- ℓ data (see, e.g., Komm et al. 2000a; Howe et al. 2004) have shown significant temporal changes in the mode heights, mode widths, and mode energies (proportional to height \times width), as previously observed by Pallé et al. (1990a,b), Jefferies et al. (1990), and Elsworth et al. (1993). All these recent studies also reported that the temporal variation of the p-mode excitation (proportional to height \times width²) is consistent with a zero change.

Here, we made use of the spatially-resolved LOWL observations obtained between beginning of 1994 and end of 1999 to carry out an independent study of the temporal variations of the p-mode damping and excitation rates with solar activity. By use of our own data anal-

ysis and peak-finding codes, we compared the observed changes for modes from $\ell = 0$ to $\ell = 99$ to the unique observations made so far at intermediate- ℓ obtained with GONG data (Komm et al. 2000a,b).

2. DATA AND ANALYSIS

2.1. Observations

The single-site helioseismic instrument LOWL, located at the Mauna Loa Solar Observatory, Hawaii (USA), has been acquiring data since February 1994. This instrument allows simultaneous observations of low- and intermediate-degree solar oscillations with spatial resolution. The LOWL instrument is a Doppler imager based on a Magneto-Optical Filter. It employs a two-beam technique to simultaneously observe the solar disk in opposite wings of the absorption line of potassium at 769.9 nm. Images are obtained every 15 sec with a spatial resolution of 25 ". The intensity difference between images obtained in both wings of the spectral line are related to the Doppler shift of the line, providing a measurement of the line-of-sight velocity of the observed area. The instrument is extremely stable against zero-point drifts and immune to noise source due to intensity fluctuations and image motions. Some of the main advantages of the instrument are its wide velocity range where the Doppler analyzer is linear, the absence of moving parts in the optics and an improved thermal control system. These attributes render it one of the best experiments for the observations of low and intermediate-degree oscillations. A more detailed description of the instrument as well as a deeper discussion of its characteristics can be found in Tomczyk et al. (1995).

The dopplergram (or velocity) images are obtained using the blue and red intensity images obtained through the two transmission bands, and were averaged over 1 minute intervals. Once the velocity images calibrated, a spherical harmonic decomposition is performed on each of them in order to create timeseries for mode degrees from $\ell = 0$ to $\ell = 99$. A spectral analysis of each of the timeseries allow us to extract the main features of the acoustic modes. Detailed explanations of the LOWL data reduction can be found in Jiménez-Reyes (2001a).

The observations used in the present analysis begin March 1st 1994 and end October 12 1999, spanning the decreasing phase and the minimum of the solar cycle 22 and the rising phase of the solar cycle 23. They were divided into 19 independent timeseries of 108 days with a 60 s cadence (Table 1), following the 36-d GONG month reference (see, e.g., Howe et al. 1999, Table 1). The duty cycles (or temporal fills) of the timeseries are very similar, about 20%, and since the observations were obtained from just one site, the timeseries present

regular gaps every 24 hours which induce temporal sidelobes, located at $\pm 11.57\mu\text{Hz}$ away from the main peak. These sidelobes were taken into account during the fitting process of the p-mode parameters (Sec. 2.2). Note also that the spectra with the 3 lowest fill values were removed for this analysis, so 16 108-d independent timeseries were used.

Table 1. Details of the 108-d LOWL timeseries

Series #	Start Date	End Date	Fill (%)	$F_{10.7}^a$	R_I^b	KPMI ^c
1	940301	940616	20	83.24	23.33	8.62
2*	940617	941002	16	80.01	27.08	8.20
3	941003	950118	23	81.44	26.92	8.77
4	950119	959596	22	82.07	25.76	8.44
5	950507	950822	23	76.85	14.48	7.99
6	950823	951208	18	74.50	15.73	7.42
7	951209	960325	22	70.49	8.37	7.06
8	960326	960711	26	71.61	8.20	6.60
9	960712	961027	20	71.32	5.82	6.40
10*	961028	970212	10	74.19	11.97	7.19
11*	970213	970531	16	74.19	12.55	6.83
12	970601	970916	21	80.26	23.82	7.68
13	970917	980102	18	92.14	34.81	9.22
14	980103	980420	30	100.26	47.08	9.75
15	980421	980806	24	111.70	61.40	11.65
16	980807	981122	18	132.51	78.01	13.43
17	981123	990310	20	140.01	72.10	14.15
18	990311	990626	23	141.61	93.28	13.90
19	990627	991012	21	161.31	97.41	15.33

^aIntegrated Solar Radio Flux at 10.7-cm, in $10^{-22}\text{W m}^{-2}\text{Hz}^{-1}$

^bSunspot Number, dimensionless

^cKitt Peak Magnetic Index, in G

Note. — The timeseries denoted by an asterisk (*) were removed for this analysis.

2.2. Mode Parameter Estimation

LOWL is an instrument with imaging capability that makes the study of a large range of solar p modes, from the low to intermediate acoustic mode degrees, possible. Due to the spherical symmetry of the Sun, the spherical harmonics are the most common of the spatial filters to isolate the information of each mode. However, the spherical harmonics are not orthogonal over the observed area, limited to half a sphere introducing correlations between different (ℓ, m) modes. Therefore, the observed power spectra, in the case of resolved observations, are a linear combination of different modes, commonly represented by the so-called leakage matrix $C_{m, m'}^{\ell, \ell'}$. It describes the imperfect isolation of the individual modes. We will discern two types of leakage signal: the spatial leaks, from same (n, ℓ) modes, and the mode contamination from different (n, ℓ) modes.

In this particular case, it can be proven that the statistics of the real and imaginary part of the Fourier transform of the (ℓ, m) modes follow a multi-normal distribution described by the so-called covariance matrix (Schou 1992; Appourchaux et al. 1998). However, as the degree of the target mode increases, the covariance matrix becomes nearly singular leading to a subsequent failure of the fitting procedure. We decided to perform a maximum-likelihood minimization using the diagonal elements of the covariance matrix to estimate the set of parameters, $\vec{a}_{n, \ell}$, describing the p-mode profiles, it is:

$$S(\vec{a}_{n, \ell}) = \sum_{m=-\ell}^{\ell} \sum_{i=1}^N \left[\ln \mathcal{M}_{n, \ell, m}(\nu_i) + \frac{Y_{n, \ell, m}(\nu_i)}{\mathcal{M}_{n, \ell, m}(\nu_i)} \right]. \quad (1)$$

The sum runs over all the points in frequency and over the $(2\ell+1)$ m -components of the multiplet. The power spectrum of the target mode is denoted by $Y_{n, \ell, m}$, while $\mathcal{M}_{n, \ell, m}$ models the power spectrum and may be written as the superposition of the spatial leaks and mode contamination, i.e.:

$$\begin{aligned} \mathcal{M}_{n, \ell, m}(\nu_i) = & \sum_{m=-\ell}^{\ell} H_{n, \ell} C_{m, m'}^{\ell, \ell} v_{n, \ell, m}(\nu) + \\ & \sum_{n', \ell', m'} H_{n', \ell'} C_{m, m'}^{\ell, \ell'} v_{n', \ell', m'}(\nu) + N_{n, \ell}, \end{aligned} \quad (2)$$

where $v_{n, \ell, m}(\nu)$ is a non-symmetric Lorentzian profile defined by:

$$v_{n, \ell, m}(\nu) = \sum_{k=-3}^3 \beta_{|k|} \frac{H_{n, \ell} (\Gamma_{n, \ell}/2)^2}{(\nu - \nu_{n, \ell, m} + k_D \times k)^2 + (\Gamma_{n, \ell}/2)^2}. \quad (3)$$

Thus, $H_{n, \ell}$, $\Gamma_{n, \ell}$, $N_{n, \ell}$ are respectively the mode height, the mode width and the background noise, while $\nu_{n, \ell, m}$ is the central frequency for each m -component of the multiplet. $\beta_{|k|}$ is the

ratio of the height of the sidelobes to the height of the main peak, estimated for each time series and k_D is the constant separation of the sidelobes, equal to $11.57\mu\text{Hz}$. Note we have taken into account the 3 first sidelobes. As observed, for example, by Duvall et al. (1993), the p-mode profiles possess small but significant levels of asymmetry: however in the case of the present analysis, the signal-to-noise ratio obtained with observations from one single-site instrument does not allow reliable estimations of the asymmetry parameter. In order to constrain the number of free parameters during the minimization process, we assumed that each m -component is well described by a non-asymmetric Lorentzian profile (eq. 3).

Regarding the central frequency for each m -component $\nu_{n,\ell,m}$, it is represented by:

$$\nu_{n,\ell,m} = \nu_{n,\ell} + \sum_{i=1}^n a_i(n,\ell)\mathcal{P}_i^\ell(m). \quad (4)$$

The polynomials $\mathcal{P}_i^\ell(m)$ are the Ritzwoller & Lavelly (1991) polynomials defined in Schou et al. (1994, App. A). The coefficients $a_i(n,\ell)$ represent the shift in frequency induced mainly by the internal rotation. The number of a -coefficients was fixed to 1 for $\ell = 1$; 4 for $\ell = 2$ and $\ell = 3$; 6 for $4 \leq \ell \leq 9$ and 9 for $\ell \geq 10$.

The mode parameters are constrained by performing simultaneous fits of the spatial leaks with the implicit assumption that the mode contamination is known. The process becomes thus iterative, improving in each iteration the mode contamination dominated (for intermediate degrees) by $n - n' = \pm 1$ and $\ell' - \ell = \pm 3$. The process is iterated until the mode frequency changes between iterations drops below a given threshold. Finally, the fits are performed inside a narrow window centered on each m -component.

Using initial guesses obtained from a collapsed diagram (Jiménez-Reyes 2001a), an iterative process was used to converge to the best estimates of the mode parameters of the 16 108-d independent series. The natural logarithms of the mode height, width, and background noise have been fitted, not the parameters themselves, resulting in a normal distribution which allows the uncertainties on each parameter to be determined from the inverse Hessian matrix.

2.3. Formulation of the Acoustic Spectrum

The mode damping rate, $\eta_{n,\ell}$, is directly related to the mode width, $\Gamma_{n,\ell}$, by:

$$\eta_{n,\ell} = \pi\Gamma_{n,\ell}. \quad (5)$$

The velocity power, or mode power, $P_{n,\ell}$, of a given mode (n, ℓ) corresponds to the area under the mode, which is a combination of the mode height, $H_{n,\ell}$, and the mode width, $\Gamma_{n,\ell}$. It can be written as:

$$P_{n,\ell} = \frac{\pi}{2} C_{\text{obs}} H_{n,\ell} \Gamma_{n,\ell}, \quad (6)$$

where C_{obs} is a constant to correct for the effects of the observational techniques. Using the analogy of the harmonic damped oscillator, the energy supplied to the modes, or energy supply rate, is estimated by:

$$\dot{E}_{n,\ell} = \frac{dE_{n,\ell}}{dt} = 2\pi E_{n,\ell} \Gamma_{n,\ell}, \quad (7)$$

where $E_{n\ell}$ is the total mode energy (Goldreich et al. 1994), which is given by:

$$E_{n\ell} = M_{n,\ell} P_{n,\ell}. \quad (8)$$

$M_{n,\ell}$ corresponds to the mode masses, which are inversely proportional to the mode inertia, $I_{n,\ell}$ (see Christensen-Dalsgaard et al. 1996).

In what follows, we focus on studying the temporal variations in the damping and the excitation rates of the p-mode oscillations. Since the peak-finding procedure returns the best estimates in natural logarithm values of the mode height and width, any temporal variations in these parameters (and any additive combinations of the two) will correspond to the fractional variations of these parameters (and any multiplicative combinations of the two). The constant C_{obs} and the mode masses, $M_{n,\ell}$, are assumed to remain constant over the solar cycle, and then can be ignored in the present analysis. Concerning the determination of the uncertainties in the variations of the mode velocity power, $P_{n,\ell}$, and the energy supply rate, $\dot{E}_{n,\ell}$, they are estimated by the formula for non-independent variables, taking into account the strong anticorrelation (taken to be equal to -0.9) between the fitted mode width, $\Gamma_{n,\ell}$, and height, $H_{n,\ell}$ (see, e.g., Chaplin et al. 2000).

Hereafter, we represent the logarithm values of $H_{n,\ell}$, $\Gamma_{n,\ell}$, $P_{n,\ell}$, and $\dot{E}_{n,\ell}$ by $h_{n,\ell}$, $\gamma_{n,\ell}$, $p_{n,\ell}$, and $\dot{e}_{n,\ell}$ respectively.

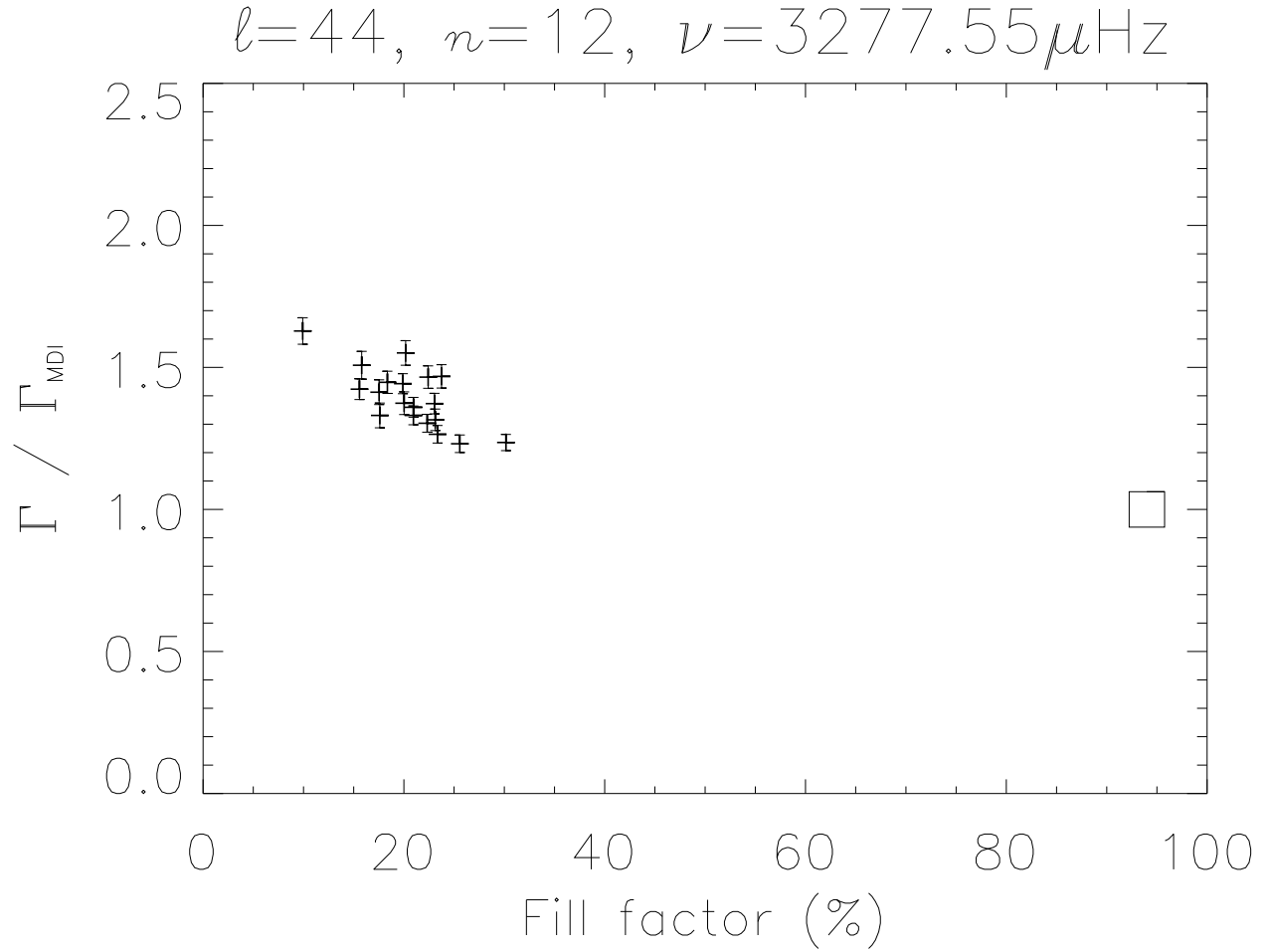


Fig. 1.— Example of the variation of the mode width, Γ , in the case of the mode $n = 12$, $\ell = 44$, as a function of the fill factor. The LOWL mode width estimates (+) were normalized by the corresponding SOHO/MDI value (\square).

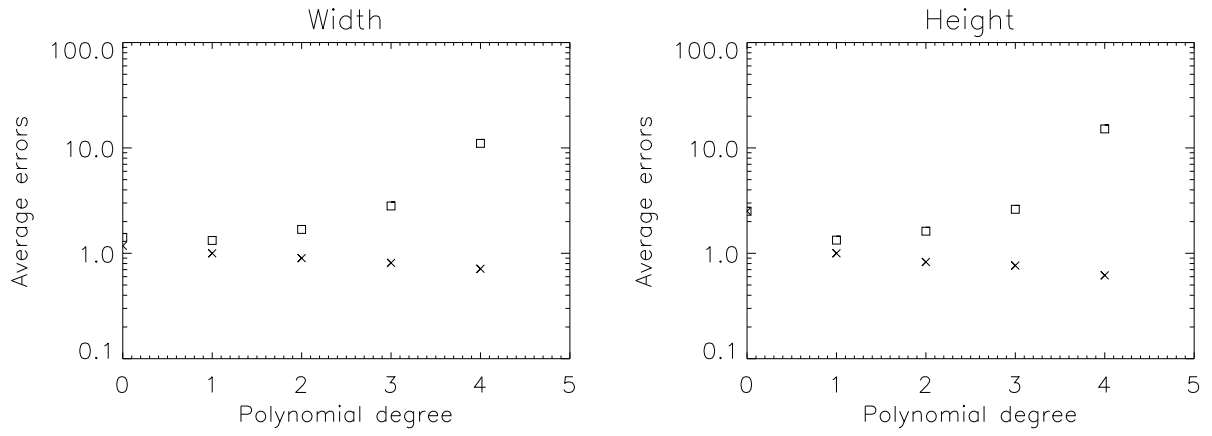


Fig. 2.— Average in-sample errors (\times) and out-sample errors (\square) of polynomial fits of the mode widths, Γ (*left panel*) and of the mode heights, H (*right panel*) as a function of the fill factor for different degrees of polynomial.

2.4. Temporal Window Correction

The presence of gaps in the observations leads to a redistribution of power from the main lobe into sidelobes and into the background. The estimates of the mode heights and of the mode widths will be then affected, the heights being underestimated and the widths overestimated. As shown in Komm et al. (2000a), the observed bias is a function of the mode degree and the mode frequency. Moreover, the effects due to the presence of gaps will be larger as the fill factor decreases.

Figure 1 shows an example of the variation in the estimation of the mode width (for $n=12$, $\ell = 44$) between a fill of nearly 100% and the actual LOWL fill factors. The plotted LOWL width estimates were normalized by the corresponding value obtained with contemporaneous timeseries from the space-based instrument SOHO/MDI, which is supposedly very close to the *true* value. Komm et al. (2000a), using GONG data, showed that a simple linear model provides an adequate description of the overestimation of the mode widths as the fill factor decreases¹, as:

$$\Gamma_i^D = c_0 + c_D \times (1 - D), \quad (9)$$

where D is the value of the fractional temporal fill; c_0 and c_D are the intercept and the gradient respectively. In that simple model, the intercept c_0 corresponds to the extrapolated width value for 100% fill, which supposes that this model is correct up to a fill of 100%. Even though this linear description is correct over a limited range of fills close to an ideal fill of 100%, it is not the case over a large range of duty cycles as we can see in Figure 1.

In this paper, we are interested in the temporal variations of the damping and excitation p-mode parameters, and not in their absolute estimates. Then, we can modify equation 9 in order to have a simple model which describes the bias from the fill factor and corrects it to the mean fill value, $\langle D \rangle$, of the analysed LOWL timeseries, instead of a 100% fill.

We also checked the degree of the polynomial necessary to describe such bias. We followed the cross-validation method described in Komm et al. (2000a) and adapted from Gershenfeld (1999) and Goutte (1997). It consists in dividing randomly our data sets into two subsets, fit one subset with the polynomial and calculate the average errors between the model and the fitted subset (also called *in-sample error*), and the average errors between the model and the excluded subset (or *out-sample error*), and repeat this procedure for several polynomial degrees. The in-sample error is expected to decrease with increasing

¹Komm et al. (2000a) also applied equation 9 to correct the observed bias from the fill factor on the other mode parameters.

model complexity, while the out-sample error will decrease up to a certain degree and then increase again when the model overfits the data. The minimum in the out-sample error as a function of the polynomial degree defines the best model.

The left panel of Figure 2 shows the corresponding results for the mode widths, and the right panel for the mode heights. The original 16 timeseries were divided into two subsets of 8 series each. On Figure 2, the average in- and out-sample errors were normalized by the in-sample error of the polynomial of degree 1. On both panels, the in-sample errors (crosses) decrease with an increasing polynomial degree, whereas the out-sample errors (squares) shows a minimum for a degree of polynomial fit equal to 1, indicating that a linear fit is the best model describing the dependence of the mode widths and heights with the fill factor.

Therefore, we decided to describe by a linear polynomial the bias introduced by the window functions on the p-mode parameters at each (n, ℓ) multiplet, but using the mean fill value, $\langle D \rangle$, instead of a 100% fill, as:

$$Y_i^D = c_0 + c_D \times (\langle D \rangle - D), \quad (10)$$

where Y_i^D stands for any of the mode parameters, where $i \equiv [h_{n,\ell}, \gamma_{n,\ell}, p_{n,\ell}, \dot{c}_{n,\ell}]$, and D is the fill factor. c_0 and c_D are again the intercept and the gradient respectively. When looking for temporal variations in the p-mode parameters, equation 10 is a sufficient description of the temporal window effects over a limited range of fill factor values. Ideally, by modulating the SOHO/MDI data with a large range of window functions between a 100% fill and fills around 20% (typical fill factor for a single-site instrument, as LOWL), we could determine an empirical model to describe the non-linear dependence between the damping and excitation p-mode parameters and the fill factors in a range from a 100% fill to lower duty cycles. This issue will be addressed in a future work.

2.5. Solar-Cycle Variations

To search for solar-cycle variations, we add to equation 10 a polynomial term function of a solar activity proxy (SAP). Then equation 10 becomes:

$$Y_i^{D,SAP} = c_0 + c_D \times (\langle D \rangle - D) + \delta Y_i^{SAP} \times SAP, \quad (11)$$

where δY_i^{SAP} is a measure of the fractional changes of each of the parameters i per unit of solar activity. The linear dependence between the p-mode parameters and solar activity has already been demonstrated by previous studies using low-degree observations (see, e.g.,

Chaplin et al. 2000; Salabert et al. 2003; Jiménez-Reyes et al. 2003) and using intermediate-degree observations (see, e.g., Komm et al. 2000a). By use of the multi-linear regression described by equation 11, we extracted the fractional temporal changes $\delta h_{n,\ell}$, $\delta \gamma_{n,\ell}$, $\delta p_{n,\ell}$ and $\delta \dot{e}_{n,\ell}$, corresponding respectively to the changes in the mode height, width, velocity power and energy supply rate, corrected from the bias due to the temporal fill. This regression was performed on the estimates of 16 108-d independent timeseries, weighted by the uncertainties returned by the peak-finding procedure, and for each mode frequency and degree. Over all the studied frequency range and mode degrees, the changes in mode parameters due to solar activity are about 3 orders of magnitude smaller than the corresponding changes due to the fill factor. Komm et al. (2000a) reported also larger effects due to the fill factor in GONG data in comparison to the effects from solar activity, but of about 1 order of magnitude. The reason for this difference of order of magnitude between LOWL and GONG observations is because the effects of the fill factor are not linear in a range from high duty cycles to lower duty cycles.

We studied these temporal variations in p-mode parameters using 3 indices of global surface activity: the Kitt Peak Magnetic Index (KPMI), obtained from the Kitt Peak magnetograms²; the Sunspot Number (R_I), and the Integrated Radio Flux at 10.7 cm ($F_{10.7}$), the two last indices obtained from the National Geophysical Data Center³. A detailed discussion about the relations among several solar activity proxies can be found in Bachmann & White (1994).

²Data available at <http://nsokp.nso.edu/>

³Data available at <http://spidr.ngdc.noaa.gov/spidr/>

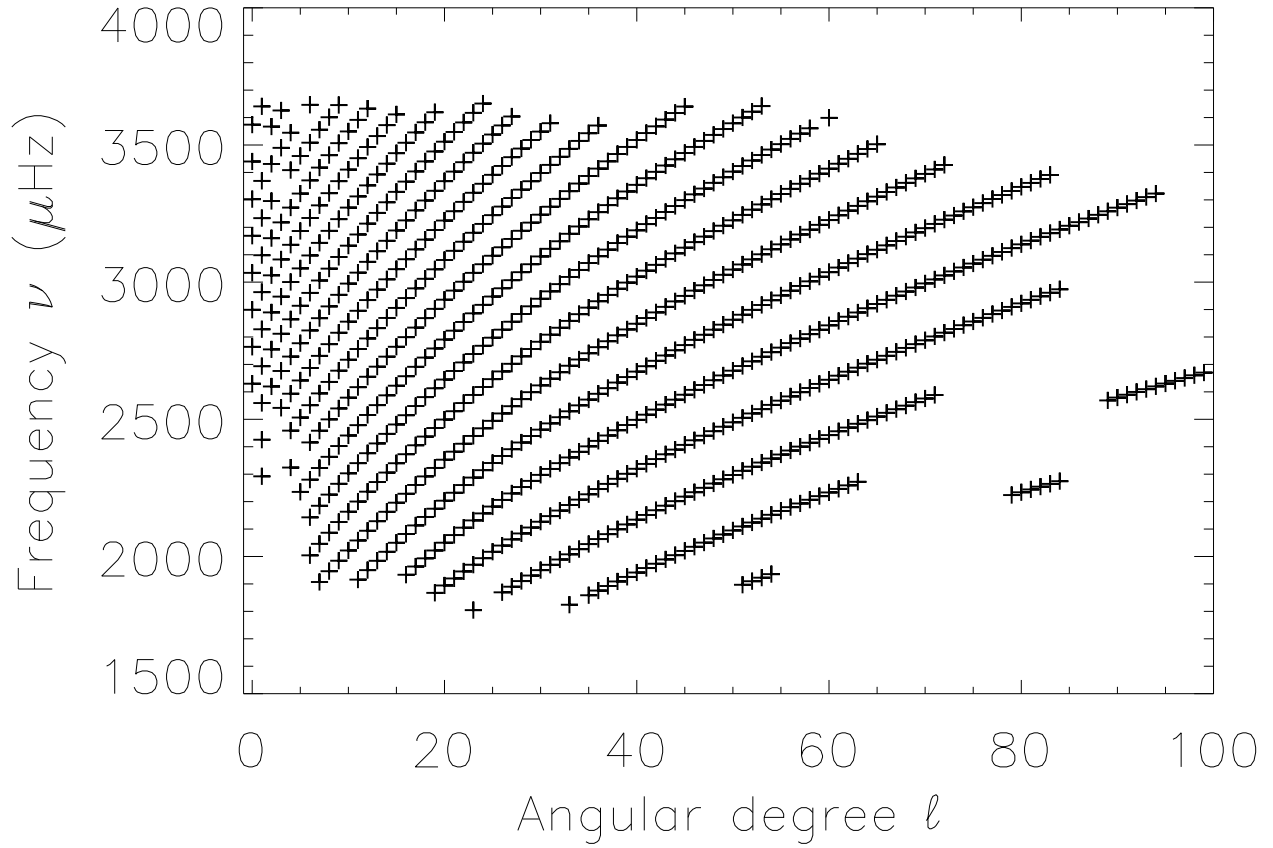


Fig. 3.— Set of common modes between the analyzed 108-d independent LOWL timeseries. The large gap of missing modes from $\ell \sim 60$ corresponds to the modes where $(\delta\nu/\delta\ell - 11.57) < 2\Gamma$.

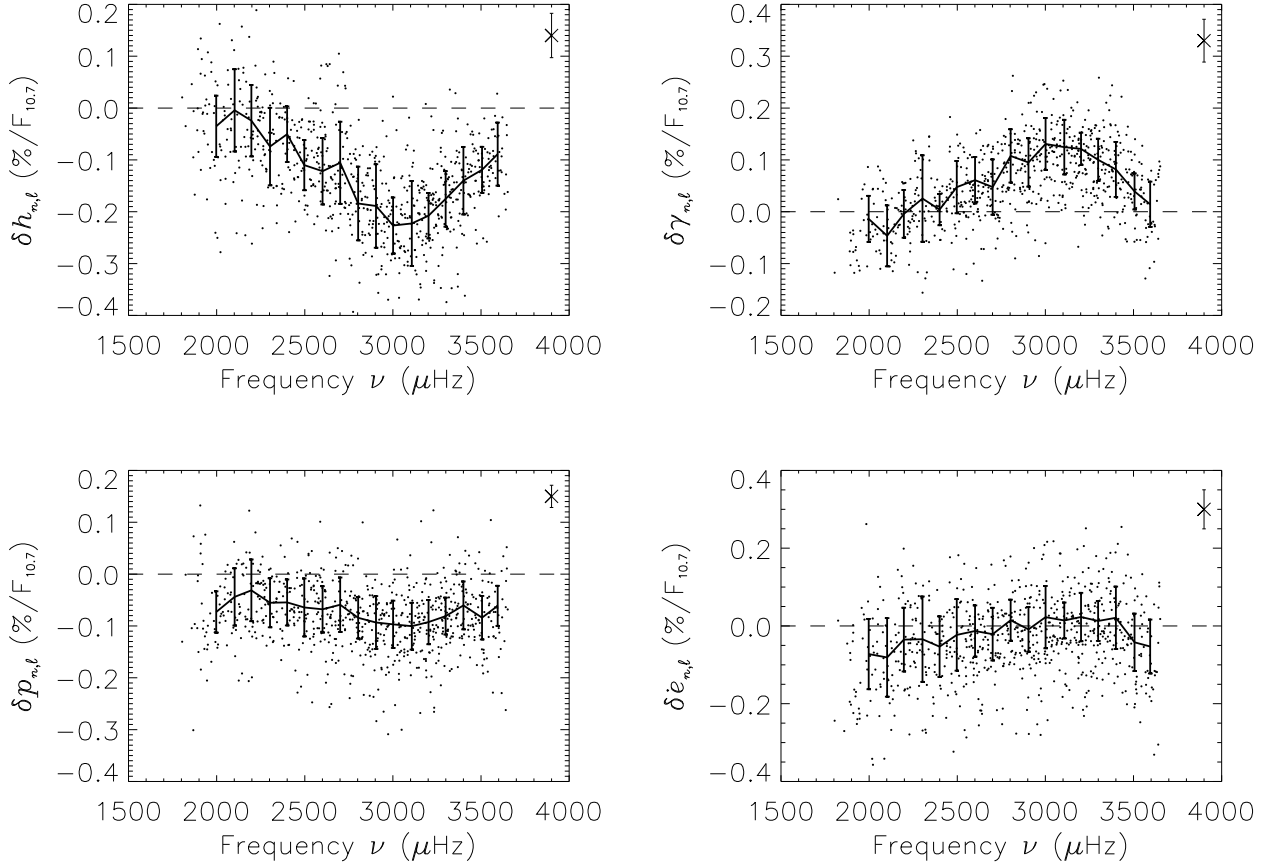


Fig. 4.— Fractional variations (% per unit of change in $F_{10.7}$) of the mode height, $\delta h_{n,\ell}$; the mode width, $\delta \gamma_{n,\ell}$; the mode velocity power, $\delta p_{n,\ell}$; and the mode energy supply rate, $\delta \dot{e}_{n,\ell}$, for $\ell = 0$ to $\ell = 99$ as a function of the frequency. The representative error bars in each upper-right panel correspond to the mean uncertainty of the fractional variations. The solid lines correspond to the averages over $30 \leq \ell \leq 60$ over frequency bins of 100 μHz , with their corresponding ± 1 standard deviations. The dashed lines represent a zero change.

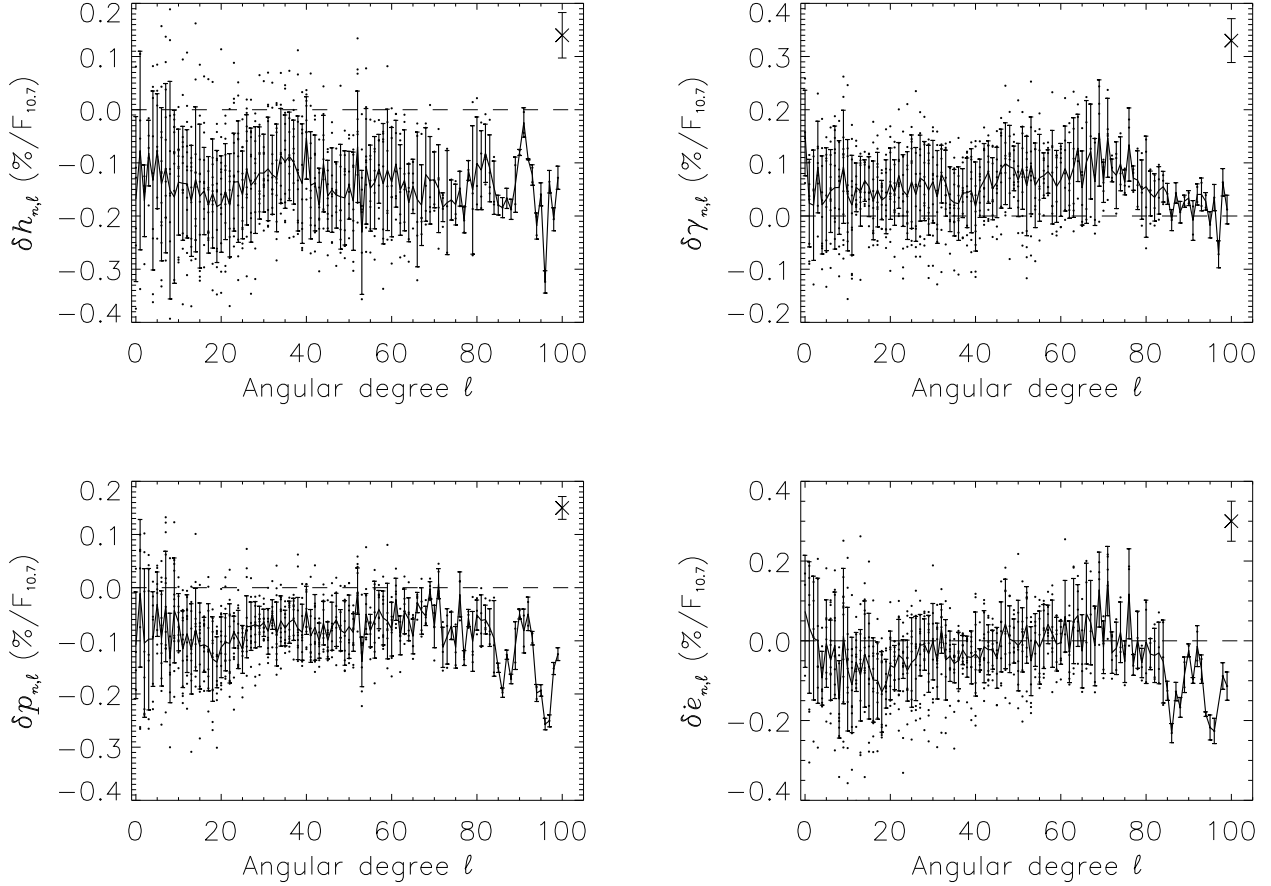


Fig. 5.— Fractional variations (% per unit of change in $F_{10.7}$) of the mode height, $\delta h_{n,\ell}$; the mode width, $\delta \gamma_{n,\ell}$; the mode velocity power, $\delta p_{n,\ell}$; and the mode energy supply rate, $\delta \dot{e}_{n,\ell}$, for $\ell = 0$ to $\ell = 99$ as a function of the mode degree. The representative error bars in each upper-right panel correspond to the mean uncertainty of the fractional variations. The solid lines correspond to the averages for each degree ℓ over the frequency range $2000 \leq \nu \leq 3500 \mu\text{Hz}$, with their corresponding ± 1 standard deviations. The dashed lines represent a zero change.

3. RESULTS

The multi-linear regression (eq. 11) was performed on the good estimates defined by a set of good-fit criteria in order to remove obvious unreasonable values, as: (1) the mode width must be within a factor of 5 of its initial guess; (2) the difference between the mode frequency and its initial guess must be less than the corresponding initial guess in mode width; and (3) the uncertainty of the mode frequency must be less than the initial guess in mode width. Moreover, in order to remove the possible systematic errors due to the blending of the leaked modes and their sidelobes into the target modes, we only kept the modes with $(\delta\nu/\delta\ell - 11.57) > 2\Gamma$. About 20% of the initial fitted modes were then removed from the estimate tables. The set of common modes used in the following analysis is composed of 771 modes (Figure 3).

Figure 4 shows the fractional changes in percent of the studied mode parameters per unit of change in the solar radio flux, $F_{10.7}$, for the mode degrees $0 \leq \ell \leq 99$ as a function of the frequency. The solid lines correspond to the averages (± 1 standard deviations) for modes between $\ell = 30$ and $\ell = 60$ over frequency bins of $100 \mu\text{Hz}$. The degree dependence of the fractional changes of the mode parameters per unit of change in $F_{10.7}$ is shown in Figure 5. The solid lines correspond to the averages (± 1 standard deviations) for each ℓ in the frequency range between 2000 and $3500 \mu\text{Hz}$. For modes with $\ell > 60$, the changes in mode height, power and energy supply rate show large fluctuations, whereas the change in mode width show a slight decrease towards zero. These changes of behaviour as a function of ℓ are most probably not related to solar activity, but rather could be the result of lower quality estimates of the parameters due to the blending of the leaked modes with the target modes, and also because of a much lower number of estimates. For these reasons, we limited all our discussions throughout this paper for modes with $\ell \leq 60$. The mean fractional changes times 10^3 per unit of change in the 3 selected solar proxies (radio flux $F_{10.7}$; sunspot number R_I ; and KPMI) are reported in Table 2 for several ranges of mode degrees and frequencies. In order to extract global changes in percent of these parameters over the solar cycle, we computed also their average changes between $30 \leq \ell \leq 60$ and $2700 \leq \nu \leq 3300 \mu\text{Hz}$, multiplied by the corresponding observed changes in the $F_{10.7}$, R_I , and KPMI indices (see Table 3).

The mode heights decrease with an increase in activity (upper-left panel on Figure 4), with a fractional change $\delta h_{n,\ell}$ of -1.30 ± 1.01 (times 10^3 per unit of change in $F_{10.7}$) over all the frequency range and between $\ell = 0$ and $\ell = 60$. $\delta h_{n,\ell}$ shows the largest variation between 2700 and $3300 \mu\text{Hz}$, with a change of -2.01 ± 0.92 (times 10^3 per $F_{10.7}$). For this range of modes, the p-mode heights change by about -25% between the minimum and the maximum of the solar cycle (see Table 3). $\delta h_{n,\ell}$ presents a strong frequency dependence, with

a maximum change centered around 3100 μHz . Even though the mode height changes are negative for all the ℓ values, with almost no ℓ -dependence, $\delta h_{n,\ell}$ decreases with decreasing ℓ -value from $\ell \sim 30$ up to $\ell \sim 20$ followed by an increase for low-degree modes (upper-left panel on Figure 5). Komm et al. (2000a) also reported a decrease in this range of ℓ -values in GONG data.

The mode widths increase with an increase in activity (upper-right panel on Figure 4), with a fractional change $\delta\gamma_{n,\ell}$ of 0.51 ± 0.77 (times 10^3 per $F_{10.7}$). As $\delta h_{n,\ell}$, $\delta\gamma_{n,\ell}$ shows the largest departure from zero in the frequency range from 2700 to 3300 μHz , with an average change of 0.94 ± 0.65 (times 10^3 per $F_{10.7}$), and presents a maximum change centered around 3100 μHz . Between the minimum and the maximum of the solar cycle, the p-mode widths increase by about 14%. The mode width changes remain positive over all the range of studied degrees (upper-right panel on Figure 5), and do not show an increase with decreasing ℓ -value as suggested by Komm et al. (2000a) with GONG observations.

The mode velocity powers exhibit a decrease with an increasing activity (lower-left panel on Figure 4), with a change $\delta p_{n,\ell}$ of -0.82 ± 0.68 (times 10^3 per $F_{10.7}$) between $\ell = 0$ and $\ell = 60$ and over all the frequency range and a largest decrease between 2700 and 3300 μHz of -1.03 ± 0.71 (times 10^3 per $F_{10.7}$). The mode power decreases by an amount of 12% over the solar cycle. Even though the frequency dependence of $\delta p_{n,\ell}$ is less important than for $\delta h_{n,\ell}$ and $\delta\gamma_{n,\ell}$, $\delta p_{n,\ell}$ presents also a maximum change around 3100 μHz . The changes in mode power are negative for all the studied ℓ values with no degree dependence for $\ell > 30$ (lower-left panel on Figure 5). However, also reported in Komm et al. (2000a), below $\ell = 30$, $\delta p_{n,\ell}$ presents the same fluctuations as $\delta h_{n,\ell}$.

The mode energy supply rates (lower-right panel on Figure 4) present a mean change $\delta\dot{e}_{n,\ell}$ of -0.41 ± 1.04 (times 10^3 per $F_{10.7}$) over all the frequency range and between $\ell = 0$ and $\ell = 60$, and of -0.21 ± 0.94 (times 10^3 per $F_{10.7}$) between 2700 and 3300 μHz . There might be some hints of a slight decrease with an increase in activity for frequencies below 3100 μHz , as already mentioned in Komm et al. (2000b). However, at the level of precision of the data, the energy supply rate is consistent with a zero change over all the studied frequency range along the solar cycle, in contrast to the other parameters which are highly frequency dependent. As a function of the mode degree, no ℓ dependence in $\delta\dot{e}_{n,\ell}$ can be observed between $\ell = 30$ and $\ell = 60$, and is consistent with a zero change (lower-right panel on Figure 5).

Similar results, summarized in Tables 2 and 3, are obtained with the sunspot number R_I , and the KPMI index. Overall, $\delta h_{n,\ell}$, $\delta\gamma_{n,\ell}$, $\delta p_{n,\ell}$ and $\delta\dot{e}_{n,\ell}$ observed with LOWL data confirm the previous observations of variations in the p-mode damping and excitation rates made at intermediate degrees obtained with GONG data (Komm et al. 2000a,b).

Even though this analysis went down as far as $\ell=0$, the precision in the observed changes for low-degree modes ($\ell \leq 3$) was such that the fractional variations were not returned at a level significant enough to perform a detailed comparison with previous results obtained with full-disk observations, which also showed no variation of the energy supply rate along the solar cycle (see, e.g., Chaplin et al. 2000; Salabert et al. 2003; Jiménez-Reyes et al. 2003). However, the low degree modes observed here show comparable amounts of changes than the intermediate degrees, at the level of precision of the data (Figure 5).

Table 2. Fractional changes $\times 10^3$ per unit change in solar activity proxy

δY_i	$F_{10.7}$				R_I				KPMI			
	$\langle \delta Y_i \rangle \pm \sigma_{\langle \delta Y_i \rangle}$	N	σ		$\langle \delta Y_i \rangle \pm \sigma_{\langle \delta Y_i \rangle}$	N	σ		$\langle \delta Y_i \rangle \pm \sigma_{\langle \delta Y_i \rangle}$	N	σ	
$0 \leq \ell \leq 60$ and $1800 \leq \nu \leq 3600$ μHz												
$\delta h_{n,\ell}$	-1.30 ± 1.01	607	-1.2		-1.31 ± 1.00	595	-1.2		-16.12 ± 10.57	596	-1.4	
$\delta \gamma_{n,\ell}$	0.51 ± 0.77	586	1.0		0.52 ± 0.75	587	1.0		7.04 ± 8.20	594	1.0	
$\delta p_{n,\ell}$	-0.82 ± 0.68	610	-1.2		-0.86 ± 0.63	605	-1.3		-9.42 ± 7.14	613	-1.3	
$\delta \dot{e}_{n,\ell}$	-0.41 ± 1.04	606	-0.4		-0.41 ± 0.97	598	-0.5		-3.10 ± 10.80	593	-0.3	
$0 \leq \ell \leq 60$ and $2700 \leq \nu \leq 3300$ μHz												
$\delta h_{n,\ell}$	-2.01 ± 0.92	225	-1.6		-2.00 ± 0.86	223	-1.6		-23.37 ± 9.14	224	-1.8	
$\delta \gamma_{n,\ell}$	0.94 ± 0.65	227	1.2		0.94 ± 0.61	227	1.2		11.73 ± 6.72	228	1.5	
$\delta p_{n,\ell}$	-1.03 ± 0.71	229	-1.4		-1.08 ± 0.66	228	-1.5		-11.73 ± 7.28	229	-1.5	
$\delta \dot{e}_{n,\ell}$	-0.21 ± 0.94	229	-0.2		-0.21 ± 0.88	228	-0.2		-1.24 ± 10.13	229	-0.1	
$30 \leq \ell \leq 60$ and $1800 \leq \nu \leq 3600$ μHz												
$\delta h_{n,\ell}$	-1.23 ± 0.95	291	-1.2		-1.26 ± 0.91	291	-1.2		-15.06 ± 9.54	291	-1.4	
$\delta \gamma_{n,\ell}$	0.57 ± 0.72	285	1.0		0.57 ± 0.70	285	1.0		7.80 ± 7.42	288	1.2	
$\delta p_{n,\ell}$	-0.71 ± 0.51	289	-1.1		-0.75 ± 0.47	289	-1.2		-7.81 ± 5.31	291	-1.1	
$\delta \dot{e}_{n,\ell}$	-0.19 ± 0.83	290	-0.2		-0.24 ± 0.80	288	-0.3		-0.50 ± 8.67	284	-0.1	
$30 \leq \ell \leq 60$ and $2700 \leq \nu \leq 3300$ μHz												
$\delta h_{n,\ell}$	-1.97 ± 0.74	105	-1.7		-1.98 ± 0.69	105	-1.7		-22.76 ± 7.32	105	-1.8	
$\delta \gamma_{n,\ell}$	1.10 ± 0.53	105	1.4		1.07 ± 0.49	105	1.5		13.17 ± 5.39	105	1.7	
$\delta p_{n,\ell}$	-0.91 ± 0.45	105	-1.3		-0.95 ± 0.42	105	-1.4		-10.09 ± 4.54	105	-1.4	
$\delta \dot{e}_{n,\ell}$	0.11 ± 0.62	105	0.1		0.04 ± 0.58	105	0.0		2.12 ± 6.57	105	0.2	

Note. — The table shows the mean fractional changes $\langle \delta Y_i \rangle$ times 10^3 per unit of change in solar activity proxy and their corresponding standard deviations $\sigma_{\langle \delta Y_i \rangle}$; the number of multiplets N ; and σ , the mean fractional changes divided by the standard deviations of the distributions of 2500 randomized data sets.

Table 3. Global changes (%) from minimum to maximum of the solar cycle averaged between $30 \leq \ell \leq 60$ and $2700 \leq \nu \leq 3300 \mu\text{Hz}$

δY_i	$F_{10.7}$	R_I	KPMI
$\delta h_{n,\ell} \dots\dots$	-23.7 ± 8.9	-26.7 ± 9.3	-25.0 ± 8.1
$\delta \gamma_{n,\ell} \dots\dots$	13.2 ± 6.3	14.5 ± 6.7	14.5 ± 5.9
$\delta p_{n,\ell} \dots\dots$	-10.9 ± 5.4	-12.9 ± 5.6	-11.1 ± 5.0
$\delta \dot{e}_{n,\ell} \dots\dots$	1.3 ± 7.5	0.5 ± 7.9	2.3 ± 7.2

Note. — The observed changes in $F_{10.7}$, R_I , and KPMI indices used in the table are 120 ($10^{-22}\text{W m}^{-2}\text{Hz}^{-1}$), 135 (dimensionless) and 11 (G) respectively.

4. SIGNIFICANCE OF THE OBSERVED CHANGES

In order to check the significance of the observed changes in the p-mode parameters, we followed the same methodology as described in Komm et al. (2000a). We randomized in time the values of the activity proxies ($F_{10.7}$, R_I and KPMI), and computed the regression using equation 11 as a function of the fill factor and the shuffled activity index. This process was repeated 2500 times, making sure to not use the same randomization twice. Figure 6 shows the distributions of the fractional changes for the mode height, mode width, mode velocity power and mode energy supply rate. They were averaged between $\ell = 30$ and $\ell = 60$ and $2700 \leq \nu \leq 3300 \mu\text{Hz}$, and normalized by the standard deviation of the distributions. The dotted lines represent the corresponding means of each distribution. The dashed lines are the averages of the real observations.

In the case of the radio flux, $F_{10.7}$, the actual average fractional changes in mode height and mode width for modes between $\ell = 30$ and $\ell = 60$ in the frequency range from 2700 to 3300 μHz are respectively -1.7 and 1.4 standard deviations of the randomized distribution away from zero, and -1.3 for the mode power. The energy supply rate is 0.1 standard deviation away from zero. The observed changes with solar activity of the mode height, mode width, and mode velocity power are then significant to about 90%, whereas the changes in mode energy supply rate is not significant, which is then consistent with a zero change. Similar results over different ranges of mode degrees and frequencies are found, and are summarized in Table 2.

As a second check, we also computed the correlation coefficients between the randomized activity indices and their corresponding real observations (see Komm et al. 2000a). The upper panels of Figure 7 show the correlation coefficients plotted versus the changes in the randomized sets for the mode height and mode width, averaged between $\ell = 30$ and $\ell = 60$ and from 2700 to 3300 μHz . The correlation in mode height and mode width show an elongated distribution along the direction of the actual observed changes (square) and centered around zero. This elongation is present also for the average over all the mode degrees and frequencies. The average randomized changes get closer to the actual change as long as the correlation between the randomized activity and the measured activity increases and gets closer to 1. Similar results are found for the changes in mode velocity power. As for the energy supply rate, the correlation coefficients are a cloud of points centered around zero, and contrary to the other parameters, do not show a preferred direction, which is consistent again with a zero change.

As a last test, and in order to check that the correction of the window function included in equation 11 does not introduce any bias in the obtained p-mode parameter changes with solar activity, we computed the correlation between the randomized activity proxies and the

fill values (see Komm et al. 2000a). The lower panels on Figure 7 present these correlation coefficients plotted versus the changes in the randomized sets for the mode height and mode width, averaged between $\ell = 30$ and $\ell = 60$ and from 2700 to 3300 μHz . No preferred directions are observed, and the points are well distributed around zero, meaning that no bias is introduced by the window function correction. The changes in mode velocity power and energy supply rate show similar clouds of points. Similar results are also obtained over different degree and frequency ranges.

We also performed the same tests with the sunspot number R_I and the KPMI index, and similar results were found (Table 2). With regard to these different tests, we can conclude that the observed changes in the p-mode damping and excitation parameters are related to solar activity. However, as for the low-degree modes ($\ell \leq 3$), their uncovered temporal variations were not observed to be statistically significant at the level of precision of the observations. Indeed, the most reliable measurements for low-degree modes come from full-disk Sun-as-a-star instruments.

In order to determine the significances of the frequency dependence reported in Section 3, the gradients on frequency were extracted by performing weighted linear fits on the 100 μHz averages from Figure 4 on both sides of 3100 μHz . The errors on the fits were used to determine the significance of the returned gradients for each of the studied parameters. As a second test, we randomized the order of the frequency values and performed the same linear regression as above on both sides of 3100 μHz on the 100 μHz averages. The process was repeated 250 times, making sure to not use the same randomization twice. The distributions of the returned gradients obtained from the randomized frequencies allowed us to measure the significances of the observed frequency dependences. Both methods return consistent results for the three solar proxies. The frequency dependences of the fractional changes in mode height, mode width and mode velocity power are significant by more than 3σ . The gradients for the mode energy supply rate are closer to 1σ , indicating that they are consistent with no frequency dependence at the level of precision of the data.

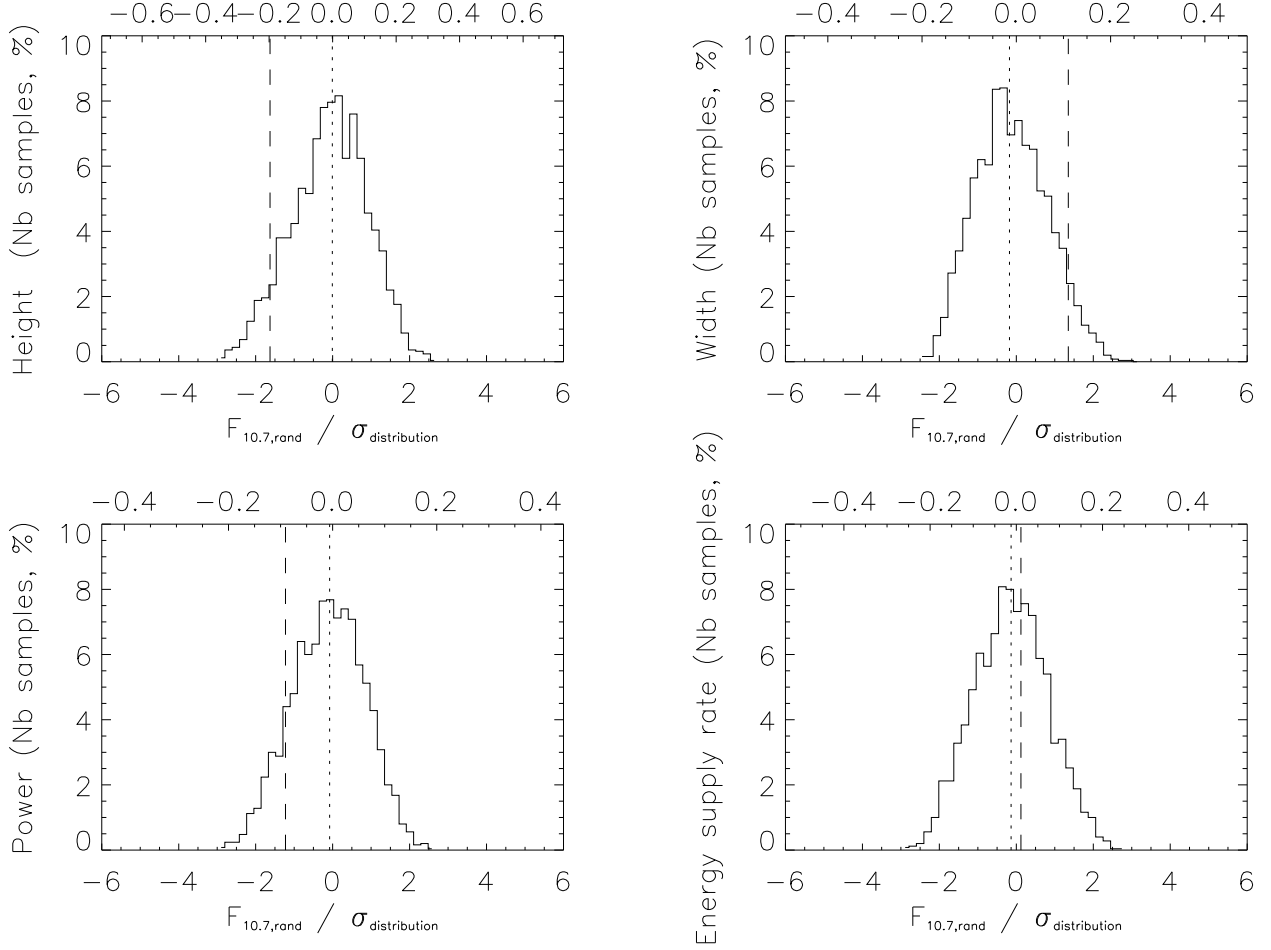


Fig. 6.— Distributions of the fractional changes in mode height, mode width, mode velocity power and mode energy supply rate (normalized by the standard deviations of the distributions, lower x -axis) obtained from 2500 randomized $F_{10.7}$ samples, averaged between $\ell = 30$ and $\ell = 60$ and $2700 \leq \nu \leq 3300 \mu\text{Hz}$. The upper x -axis are in the actual observed change units. The dotted lines correspond to the means of the distributions, and the dashed lines to the actual observations (Figures 4-5).

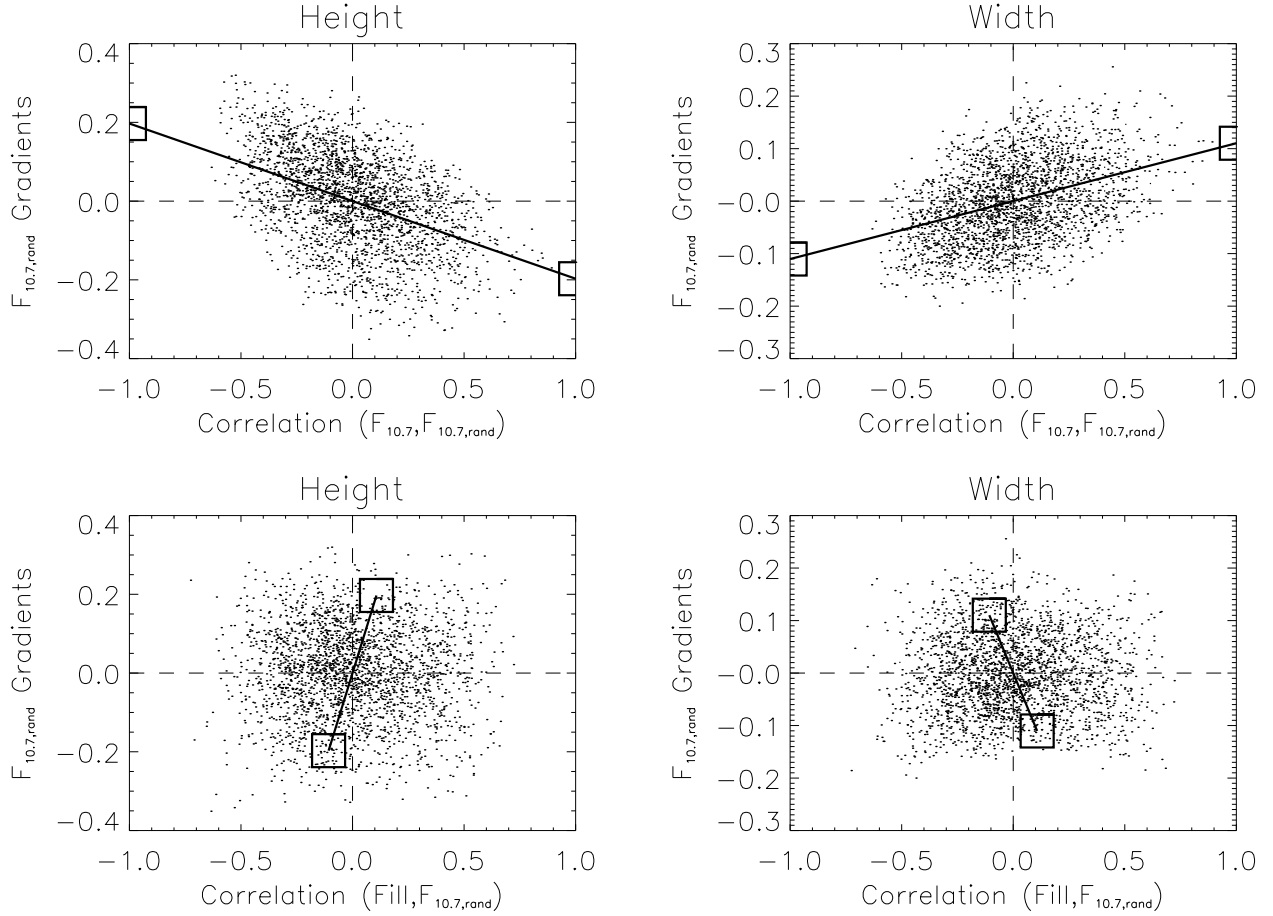


Fig. 7.— Fractional changes in mode height and mode width obtained from 2500 randomized $F_{10.7}$ samples as a function of the correlation coefficients between the measured and randomized radio flux (*upper row*) and between the fill value and the randomized radio flux (*lower row*), averaged between $\ell = 30$ and $\ell = 60$ and $2700 \leq \nu \leq 3300 \mu\text{Hz}$. The squares connected by a solid line correspond to the actual values.

5. SUMMARY AND DISCUSSION

We used the LOWL observations collected between beginning of 1994 and end of 1999 to study the temporal variations of the p-mode damping and excitation parameters with solar activity over a wide range of angular degrees. We extracted the temporal variations in mode height, mode width, mode velocity power and mode energy supply rate by applying a multi-linear regression (eq. 11) on the estimates of 16 108-d independent timeseries. This regression allowed us to correct the bias on the peak-finding estimates from the temporal fills and to obtain a measure of their fractional changes. We showed that the p-mode damping and excitation parameters between $\ell = 0$ and $\ell = 60$ present different behaviours with solar activity. Similar results are obtained with 3 different solar activity proxies (the integrated solar radio flux, $F_{10.7}$; the sunspot number, R_I ; and the Kitt Peak Magnetic Index, KPMI). Our findings confirm the previous measurements at intermediate- ℓ modes obtained with GONG observations (Komm et al. 2000a,b).

The mode heights decrease with increasing activity and show the largest variations among the mode parameters. The p-mode damping (proportional to the mode widths) shows an increase with an increasing activity. Just as with the mode heights, the mode velocity power decreases with an increasing activity. Their sensitivities to solar activity show clear evidence of a frequency dependence, the modes in the frequency range from 2700 to 3300 μHz showing the largest variations and presenting a maximum change centered around 3100 μHz , as already reported in GONG observations (Komm et al. 2000a). In contrast to the other parameters, the p-mode excitation does not show a significant frequency dependence and is consistent with a zero change along the solar cycle.

As a function of the mode degree, the variations in the damping and excitation p-mode parameters are more or less ℓ -independent over the range of studied degrees as observed by Komm et al. (2000a) with GONG data. However, in the limit of precision of the data and as already mentioned in Komm et al. (2000a), there might be some hints of a decrease in the changes in mode height, mode velocity power and mode energy supply rate for $\ell < 30$, while the mode damping variations do not present an increase with decreasing ℓ -value as suggested by Komm et al. (2000a).

The relative sizes of the uncovered changes at intermediate ℓ are consistent with an increase of the damping rate over the solar cycle, while the net forcing of the modes remains constant. Then, in the description of the p modes by a damped, forced oscillator, the sizes and signs they uncovered can result from changes only to the net damping, as already pointed out by Chaplin et al. (2000) for low- ℓ modes.

Our findings about the energy supply rate are consistent with the results obtained with

GONG data (Komm et al. 2000b), showing no significant changes in the p-mode excitation with solar activity, but we cannot rule out that the energy supply rate might change locally, since the peak-finding procedure used in this analysis minimized only one height and one width per each (ℓ, m) multiplet. However, Komm et al. (2002) stated that "within the limits of the current measurements (i.e., GONG observations), the energy supply rate does not sense the latitudinal distribution of magnetic activity".

This work was supported by NSF through base funding of HAO/NCAR and partially funded by the grant AYA2004-04462 of the Spanish National Research Plan. The authors acknowledge the LOWL observers Eric Yasukawa and Darryl Koon. NSO/Kitt Peak magnetic data used here are produced cooperatively by NSF/NOAO, NASA/GSFC and NOAA/SEL.

REFERENCES

- Appourchaux, T., Gizon, L., & Rabello-Soares, M.-C. 1998, *A&AS*, 132, 107
- Bachmann, K. T., & White, O. R. 1994, *Sol. Phys.*, 150, 347
- Chaplin, W. J., Elsworth, Y., Isaak, G. R., Lines, R., McLeod, C. P., Miller, B. A., & New, R. 1998, *MNRAS*, 300, 1077
- Chaplin, W. J., Elsworth, Y., Isaak, G. R., Miller, B. A., & New, R. 2000, *MNRAS*, 313, 32
- Christensen-Dalsgaard, J., et al. 1996, *Science*, 272, 1286
- Duvall, T. L., Harvey, J. W., Libbrecht, K. G., Popp, B. D., & Pomerantz, M. A. 1988, *ApJ*, 324, 1158
- Duvall, T. L., Jr., Jefferies, S. M., Harvey, J. W., Osaki, Y., & Pomerantz, M. A. 1993, *ApJ*, 410, 829
- Elsworth, Y., Howe, R., Isaak, G. R., McLeod, C. P., Miller, B. A., Speake, C. C., Wheeler, S. J., & New, R. 1993, *MNRAS*, 265, 888
- Gelly, B., Lazrek, M., Grec, G., Ayad, A., Schmider, F. X., Renaud, C., Salabert, D., & Fossat, E. 2002, *A&A*, 394, 285
- Gershenfeld, N. 1999, *The nature of mathematical modeling* / Neil Gershenfeld. Cambridge ; New York : Cambridge University Press, 1999
- Goldreich, P., Murray, N., & Kumar, P. 1994, *ApJ*, 424, 466

- Goutte, C. 1997, *Neural Computation*, 9, 1245
- Howe, R., Komm, R., & Hill, F. 1999, *ApJ*, 524, 1084
- Howe, R., Komm, R. W., Hill, F., Haber, D. A., & Hindman, B. W. 2004, *ApJ*, 608, 562
- Komm, R. W., Howe, R., & Hill, F. 2000a, *ApJ*, 531, 1094
- Komm, R. W., Howe, R., & Hill, F. 2000b, *ApJ*, 543, 472
- Komm, R., Howe, R., & Hill, F. 2002, *ApJ*, 572, 663
- Libbrecht, K. G., & Woodard, M. F. 1990, *Nature*, 345, 779
- Jefferies, S. M., Duvall, T. L., Harvey, J. W., & Pomerantz, M. A. 1990, *LNP Vol. 367: Progress of Seismology of the Sun and Stars*, 367, 135
- Jiménez-Reyes, S. J., Régulo, C., Pallé, P. L., & Roca Cortés, T. 1998, *A&A*, 329, 1119
- Jiménez-Reyes, S. J. 2001a, Ph.D. Thesis,
- Jiménez-Reyes, S. J., Corbard, T., Pallé, P. L., Roca Cortés, T., & Tomczyk, S. 2001b, *A&A*, 379, 622
- Jiménez-Reyes, S. J., García, R. A., Jiménez, A., & Chaplin, W. J. 2003, *ApJ*, 595, 446
- Pallé, P. L., Régulo, C., & Roca Cortés, T. 1990a, *LNP Vol. 367: Progress of Seismology of the Sun and Stars*, 367, 189
- Pallé, P. L., Régulo, C., & Roca Cortés, T. 1990b, *LNP Vol. 367: Progress of Seismology of the Sun and Stars*, 367, 129
- Ritzwoller, M. H., & Lavelly, E. M. 1991, *ApJ*, 369, 557
- Salabert, D., Jiménez-Reyes, S. J., Fossat, E., Gelly, B., & Schmider, F. X. 2002, *ESA SP-508: From Solar Min to Max: Half a Solar Cycle with SOHO*, 11, 95
- Salabert, D., Jiménez-Reyes, S. J., & Tomczyk, S. 2003, *A&A*, 408, 729
- Schou, J. 1992, Ph.D. Thesis,
- Schou, J., Christensen-Dalsgaard, J., & Thompson, M. J. 1994, *ApJ*, 433, 389
- Thompson, M. J., Christensen-Dalsgaard, J., Miesch, M. S., & Toomre, J. 2003, *ARA&A*, 41, 599

Tomczyk, S., Streander, K., Card, G., Elmore, D., Hull, H., & Cacciani, A. 1995, *Sol. Phys.*,
159, 1

Woodard, M. F., & Noyes, R. W. 1985, *Nature*, 318, 449